Influence of Clumps-Weighted Moorings on a Spar Buoy Offshore Wind Turbine

Niccolo Bruschi *, Giulio Ferri [ID]**, Enzo Marino** [ID] **and Claudio Borri**

Department of Civil and Environmental Engineering, University of Florence,
Via Santa Marta 3, 50139 Firenze, Italy; giulio.ferri@unifi.it (G.F.); enzo.marino@unifi.it (E.M.);
claudio.borri@unifi.it (C.B.)
* Correspondence: niccolo.bruschi@unifi.it

check for
updates

Abstract: The spar buoy platform for offshore wind turbines is the most utilized type and the OC3 Hywind system design is largely used in research. This system is usually moored with three catenary cables with 120° between each other. Adding clump weights to the mooring lines has an influence on the platform response and on the mooring line tension. However, the optimal choice for their position and weight is still an open issue, especially considering the multitude of sea states the platform can be exposed to. In this study, therefore, an analysis on the influence of two such variables on the platform response and on the mooring line tension is presented. FAST by the National Renewable Energy Laboratory (NREL) is used to perform time domain simulations and Response Amplitude Operators are adopted as the main indicators of the clump weights effects. Results show that the clump weight mass is not as influential as the position, which turns out to be optimal, especially for the Surge degree of freedom, when closest to the platform.

Keywords: offshore wind energy; spar buoy floating platform; mooring lines; clump weights

1. Introduction

Wind turbines are used as alternative energy harvesters in order to reduce CO_2 emissions. In particular, the offshore sector is being largely explored because of its higher wind potential compared to the onshore one. The offshore wind energy has an estimated technical potential of 192,800 TWh/yr [1]. Especially in deep water, the atmospheric conditions are more profitable in comparison with coastal areas so offshore wind farms have been more widely employed in recent years. Unfortunately, deep water areas do not allow for fixed bottom-type wind turbines, due to the unsustainable cost of the foundation. Thus, floating offshore wind turbines play a key role at the moment, allowing an increase in the siting possibilities for offshore wind energy plants by exploiting areas characterized by deep water (e.g., the Mediterranean Sea). Nowadays, the majority of offshore wind turbines installed in Europe are placed in shallow water [2]. The average distance to shore (59 km) and water depth (33 m) continue to increase even though most wind farms are bottom-fixed [3]. Moreover, Europe's floating wind fleet is the largest worldwide (70%) with a total of 45 MW by the end of 2019 [3]. Floating wind turbines are a future key of the European wind energy sector, allowing the exploitation of deep water sites, such as those available in the Mediterranean Sea.

Different typologies of floating platform have been proposed worldwide [4,5]. They include the spar [6–10], Tension Leg Platform (TLP) [11,12], Semi-Submersible Platform [13,14], among others. In October 2017 the first floating offshore wind farm was built by Statoil, by employing spar-buoy platforms, which, since then, has been the most utilized technology in the whole floating offshore sector. Numerous research contributions have been delivered in recent years focusing on this platform type [7,15–18], and several optimization approaches have been adopted [19]. These studies aim at

improving the platform behavior by modifying the structure itself [18,19], the number of mooring lines [15], or by studying the effects of different clump weight configurations under the wave and the wind effects as done Liu et al. [17]. Many codes, such as the National Renewable Energy Laboratory (NREL) FAST [20], HAWC2 [21], etc., have been used for the simulation of the OC3-Hywind spar platform. This type of platform is connected to the bottom of the sea through three catenary cables. Barbanti et al. [22] showed, using a genetic algorithm optimization, that the platform response is almost insensitive to the mooring line geometry, while the use of clump weights can reduce the fatigue load and improve the overall system response. Yuan et al. [23] studied a hybrid mooring system with clump weights on the bottom part of the cable and buoy near the platform. The analysis focused on the optimization of the buoy's position and volume based on the mooring line tension for a semisubmersible platform. Hordvik [24] analyzed optimized mooring line configurations for the OC3 Hywind spar platform, focusing on the minimization of the mooring line tension. Most of the studies regarding the spar buoy-type platform [22–24] have been performed using the strip-theory approach, which is based on Morison's equation [25].

The aim of this work is to optimize the mooring system of a spar-buoy floating wind turbine incorporating clump weights via time-domain simulations. The studies mentioned above are focused on specific load cases and they analyze platform response and mooring lines separately. Thus, the purpose of the present work is to find a reliable method to analyze both platform response and cable tension, independently from specific sea states. The structural response is obtained using FAST [20]. The assessment of the system response is made considering the platform Response Amplitude Operators (RAOs) of pitch and surge motion of the platform, and the mooring line tension. The position and weight of the clump weights are the two design variables considered. In addition, the mean value of the cable tension at the fairlead is considered.

In Section 2 the methodology adopted is presented. In Section 3, first some preliminary simulations and results are described in order to verify the method, then the influence of the design variables is discussed and an optimal configuration is identified. Finally, in Section 4, the main conclusions are drawn.

2. Methodology

The present work focuses on one of the most used spar-buoy platforms in the literature: the OC3-Hywind spar-buoy. The NREL 5-MW baseline wind turbine [26] along with the OC3 Hywind platform [6] is investigated using FAST, a fully coupled hydro–aero–servo–elastic time-domain simulator developed and validated by means of experimental analyses (see for example [27]), by the National Renewable Energy Laboratory [20].

In this section, first a description of the OC3-Hywind characteristics is presented, followed by the model used in the simulations. Then, Response Amplitude Operators (RAOs) are introduced and results of preliminary analyses are discussed.

2.1. OC3-Hywind Spar-Buoy Floating Wind Turbine Description

Wind turbine, platform and mooring system properties are chosen according to the description provided by the Offshore Code Comparison (OC3) study for the Hywind concept [6]. This model is derived from the first floating wind turbine installed in the world (Statoil Hywind 2.3 MW-scale prototype installed in Norway in 2009). This model is largely used in the research field due to the fact that it has been modified to create a benchmark case for code comparison. The OC3 Hywind is a spar buoy-type wind turbine with three slack catenary mooring lines and it is equipped on the top with the NREL 5 MW offshore reference wind turbine [26], which is also largely adopted as a benchmark model for the comparison of different simulation tools. The platform is made by two cylindrical columns with different diameters connected by a conic element [6]. The smaller cylinder is about 10 m long, which is the platform draft over the still water level needed. The OC3-Hywind properties are listed in Table 1.

**Table 1.** OC3-Hywind concept specifications [6].

Tower top height above SWL (Sea Water Level)	87.6 m
Tower Mass	249,718 kg
Platform total draft	120 m
Platform draft above SWL	10 m
Platform mass	7,466,330 kg
Platform diameter above taper	6.5 m
Platform diameter below taper	9.4 m
Taper depth below SWL	4–12 m
CM Location Below SWL Along Platform Centerline	89.9155 m
Platform Roll Inertia about CM (Center of Mass)	4,229,230,000 kgm^2
Platform Pitch Inertia about CM	4,229,230,000 kgm^2
Platform Yaw Inertia about Platform Centerline	164,230,000 kgm^2

Regarding the mooring lines, the connection to the platform is made with the delta line, which is modeled by adding a yaw stiffness contribution. The mooring lines specifications are listed in Table 2.

Table 2. OC3-Hywind mooring system specifications [6].

Number of mooring lines	3
Angle between adjacent lines	120°
Depth to Anchors Below SWL (Water Depth)	320 m
Depth to Fairleads Below SWL	70 m
Radius to Anchors from Platform Centerline	853.87 m
Radius to Fairleads from Platform Centerline	5.2 m
Unstretched Mooring Line Length	902.2 m
Mooring Line Diameter	0.09 m
Equivalent Mooring Line Mass Density	77.7066 kg/m
Equivalent Mooring Line Extensional Stiffness	384,243 kN
Additional Yaw Spring Stiffness	98,340,000 Nm/rad

To model the mooring lines, FAST provides two different modules called MAP and MoorDyn [28]. While MAP is a static model which ignores the inertia forces and fluid drag loads, MoorDyn is a dynamic, multi-segmented, lumped-mass module. In general, both models can be used in different situations. However, given the important role that more accurate mooring line models have [29,30], in the present study MoorDyn is used. In Figure 1 there is shown a simple scheme of the platform and one of its mooring lines attached with a clump weight.
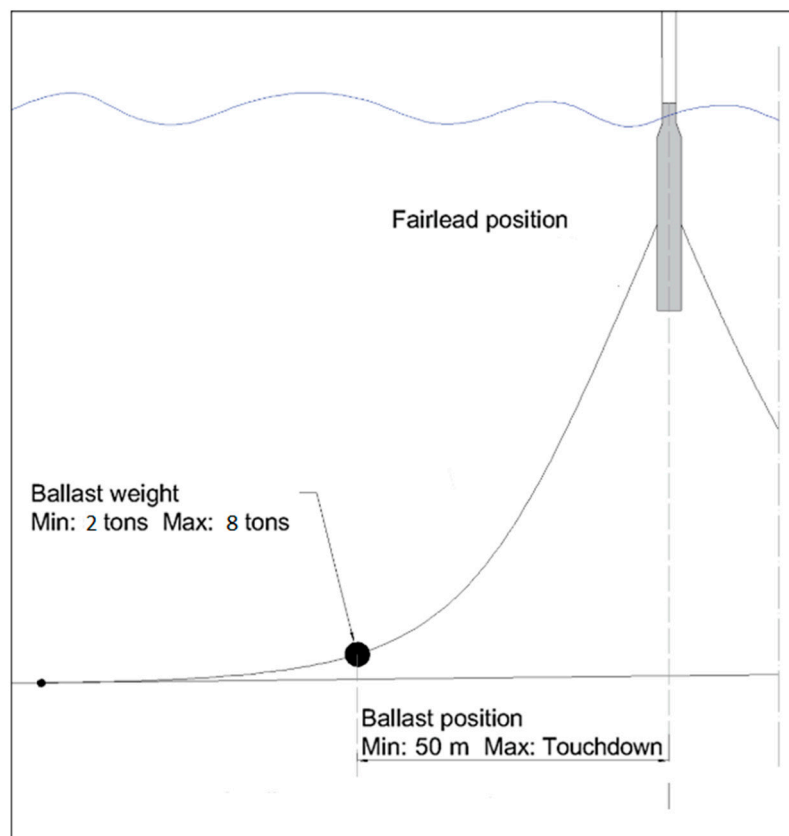
Figure 1. Scheme of the substructure system, platform plus mooring line (rearranged from [22]).

2.2. Hydrodynamic Model

HydroDyn [31] is the hydrodynamic module in FAST responsible for the analysis of the hydrodynamic loads on the platform. HydroDyn allows multiple approaches for calculating the hydrodynamic loads on a structure: a potential-flow theory solution, a strip-theory solution and a hybrid-combination of the two [32].

The potential-flow theory, which is the one adopted in the present study (as opposed to [22], where the strip-theory was employed), is the most comprehensive approach used in HydorDyn and involves frequency-to-time-domain transformations. It requires the definition of the hydrostatic restoring coefficients, the added mass and damping contributions from linear wave radiation, and the incident-wave excitation (Froude–Krilov forces). These required hydrodynamic coefficients are frequency-dependent and, in general, must be provided by an external frequency-domain panel-based code. However, the OC3 Hywind test case provided by NREL includes all the hydrodynamic data obtained with the external software WAMIT [33]. More accurate models capable to account for important nonlinear effects, see for example [34–39] for fixed bottom platforms and [40–43] for floating platforms, should be used for higher fidelity simulations. However, when high efficiency is required as in the present case, the potential-flow theory together with the assumption of small waves and small body motion represent an acceptable trade-off between accuracy and efficiency. It is noted that purely frequency domain models [18,44,45] are even more appealing due to their higher efficiency.

In the following, the essential assumptions of the hydrodynamic model used in this work are briefly recalled. Further details are available in [46].

- The fluid is assumed to be inviscid and incompressible; the flow irrotational. These assumptions ensure the existence of a velocity potential, which is a function of time and space.

- Small amplitude waves and small displacements/rotations of the floating body. These assumptions permit linearizing the dynamic free surface boundary condition and simplifying the kinematic boundary condition at the body.
- Steady-state condition. The velocity potential can be written isolating the time dependence and the space dependence. The space-depending part can be divided in two components which are solutions of two different Boundary Value Problems (BVPs): diffraction (platform in static condition and wave motion) and radiation (platform motion with no waves). Moreover, the diffraction potential can be divided, due to the linearity assumption, into incident and scattering wave potentials.

Finally, the dynamic pressure is calculated by means of the linearized Bernoulli equation, and added mass matrix, damping matrix and hydrodynamic forces are obtained integrating such a pressure field.

2.3. Response Amplitude Operator

The time-domain analysis performed by FAST provides the system response under the wind and waves forcing loads. To assess the system response independently from the specific environmental conditions, Response Amplitude Operators (RAOs) are used. For a given Degree Of Freedom (DOF), the RAO is defined as the ratio of the cross-spectral density of the input and the auto-spectral density of the corresponding output:

$$RAO = \sqrt{\frac{S_{xy}(\omega)}{S_{xx}(\omega)}} \tag{1}$$

where, $S_{xy}(\omega)$ and $S_{xx}(\omega)$ are the cross-spectral and auto-spectral densities of the input $x(t)$ and the output $y(t)$, in the frequency domain, respectively. In this work the pitch and the surge motion of the platform, as well as the cable tension at the fairlead, are the DOFs considered. The water surface elevation is used as forcing input, obtained with a white noise spectrum characterized by a significant wave height of 2 m, i.e., small enough to adopt a linear wave theory in the range of frequencies between 0 and 0.25 Hz. All simulations performed are carried out in absence of wind and with the blades pitch set at 0°. This condition makes the waves the only input to the system, and permits focusing only on the wave–structure interaction. Due to the absence of wind, the aero–servo–elastic effects of the rotor were not considered. For all analyses, the simulation time is 8000 s, cutting off the first 2000 s. The time step is 0.025 s, which is sufficiently small for accurate time domain results and associated spectral analyses.

3. Results

3.1. Simulation without Clump Weights

Six simulations, each with a different seed for the withe noise sea spectrum, without clump weights are performed. Then, from the time histories of the platform response, the auto-spectral density of the input (wave elevation) and the cross-spectral density of the input/output (system responses) are evaluated. The six spectral densities mean value is used to obtain the RAOs. In order to verify the present result, a comparison is made with the results obtained by Ramachandran et al. [47].

RAOs of surge, pitch, and heave DOFs are shown in Figure 2.
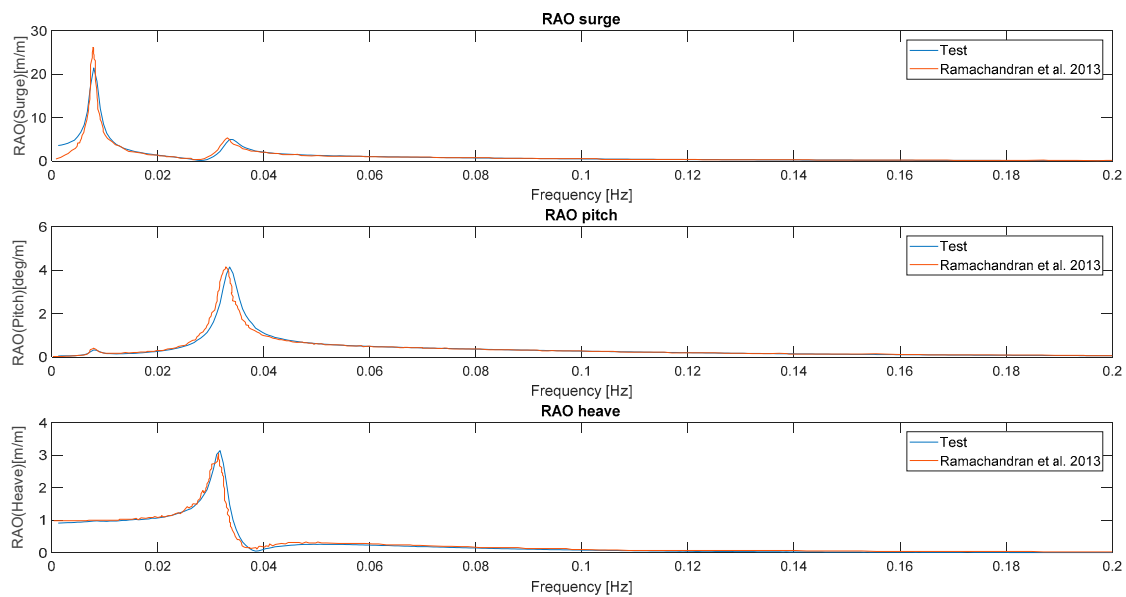
Figure 2. OC3 Hywind Response Amplitude Operator (RAO) comparison with Ramachandran et al. [47] for a test with no clump weights (no wind, white noise sea state).

Figure 2 shows a very good agreement with [47]. The peak of the surge RAO is lower than the reference one due to the random nature of the seeds used to create the white noise. Once an overall verification of the present results is assured, the influence of the clump weights on the structural response of the platform is analyzed. In contrast to the previous case, for a more realistic simulation, the following analyses are performed with a non-zero transverse viscous drag coefficient for the mooring lines [6], namely it is assumed Cd = 1.6. Such a value is chosen according to the NREL certified test for the OC3 Hywind. Importantly, it is noted that viscous drag contribution significantly affects the surge motion, and both the clump weight and the cable damping cause a remarkable decrease in the peak of the surge RAO. Moreover, it is noted that adding a clump weight on the cables changes the overall floating stability of the platform. The reference model of the OC3 Hywind is designed with a specific draft. To maintain this value unchanged with the added mass on the cable the following procedure is used. Once mass and position of the clump weight are set, a short (but sufficiently long) simulation is run to provide information about the change in the fairlead tension. This tension, in its vertical component, can be balanced by the buoyancy of the platform. Thus, the ballast at the bottom part of the platform is reduced at the beginning of every simulation, in order to keep the requested draft unchanged. After this ballast adaptation procedure, the actual simulation is performed for a duration of 8000 s.

3.2. Simulation with Clump Weights

Surge and pitch RAOs are then evaluated for various combinations of mass and position of the weight along the cable. Heave motion was not considered because clump weights have negligible effect on this DOF [22]. As shown in Figure 3, the natural frequencies do not change using different weights at different positions; in contrast, peaks at the natural frequency vary from case to case. The results (Figure 3a top panel) show an influence in the surge motion reducing the peak at the natural frequency from 26 to about 15. The effects of the cable viscous drag bring the RAO surge peak to 16 (compare the cyan curve with the case with no clump weights and no cable viscous drag in Figure 2). Thus, the effect of clump weights is less impactful if the result of Figure 3 is compared with this value instead to the one of Ramachandran et al. [47]. The clump weight position gives a not negligible decrease in the surge motion, bringing its RAO peak to 12.6 in the position close to the platform (x = 50 m, see blue curve in Figure 3a, upper plot). Regarding the influence of weight and position, a clump weight closer

to the platform implies a lower RAO peak in surge motion, while the weight (Figure 3b top panel) has no noticeable influence on it. In terms of pitch motion the results show that both position (Figure 3a bottom panel) and weight (Figure 3b bottom panel) of the ballast do not influence the RAO peak, while the presence of the clump weight still has a positive impact on it, reducing the peak from 4.2 to 3.8.

(**a**)

(**b**)
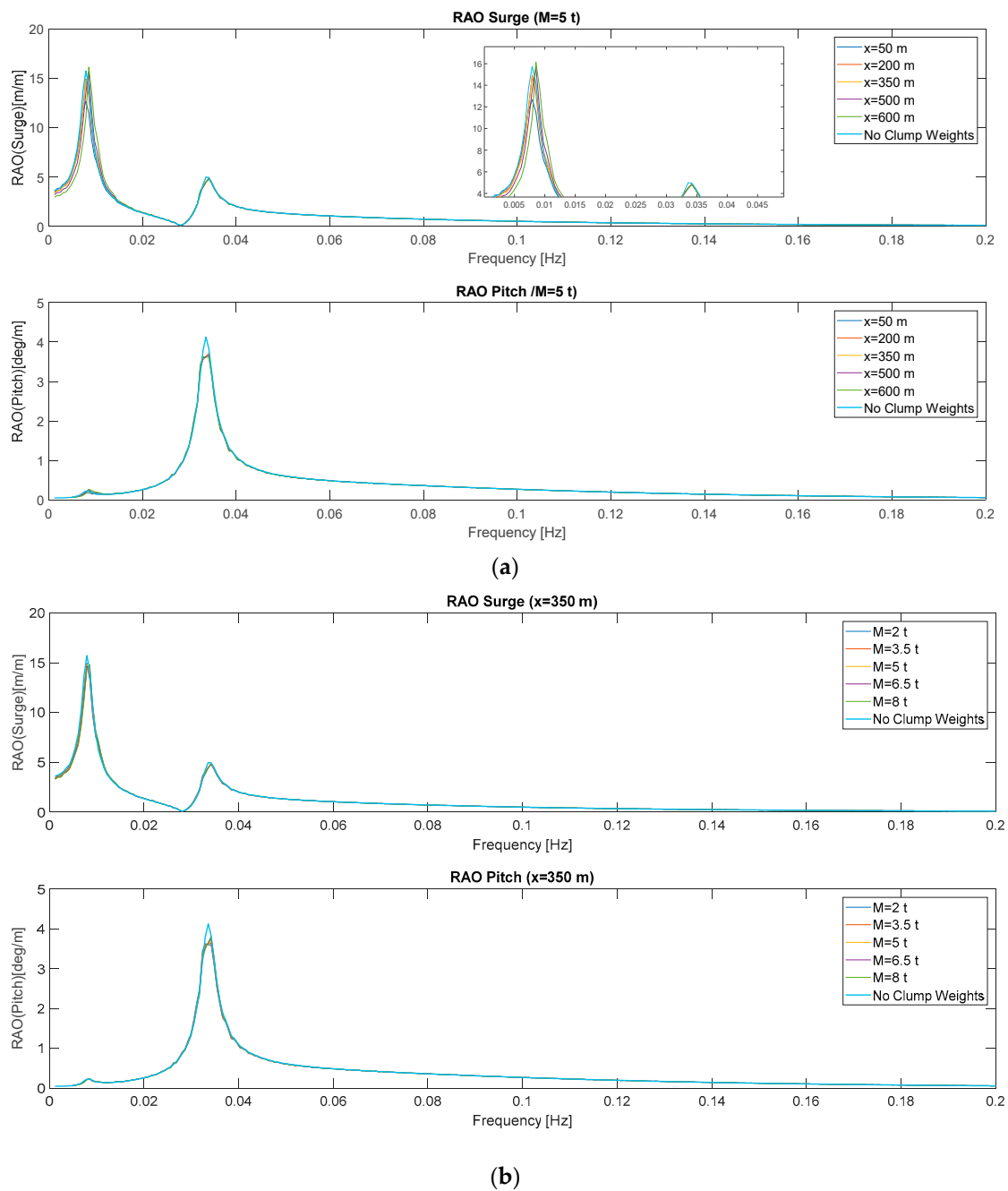
Figure 3. Pitch and Surge RAOs for different positions (**a**) and weights (**b**) of the cable ballast.

Besides indications on the trend, these preliminary results do not give a complete picture of the simultaneous effects of the two variables. Therefore, the same variables are analyzed with surface graphs (Figure 4).
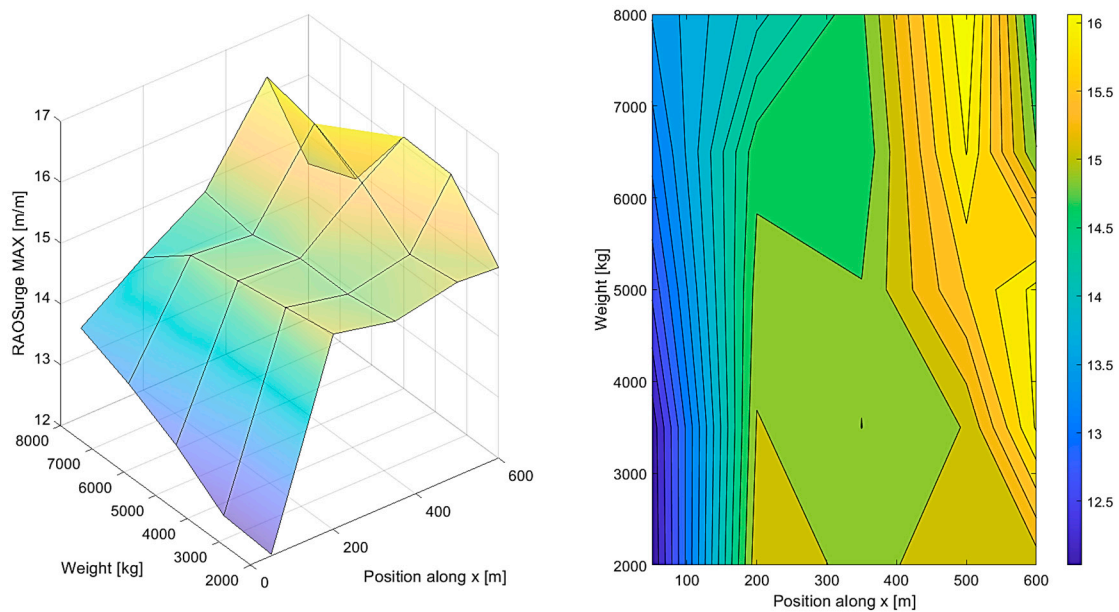
**Figure 4.** Peak of the Surge motion's RAO using 5 different positions and 5 different masses.

Figure 4 shows how the peak of the surge RAO behaves for different combinations of weight and its position. It appears clear that a small weight and a position of the ballast close to the platform give the lowest value of the surge RAO peak. A minimum of 12.3 is found at a position of 50 m with a mass of 2 t. The optimal combination of weight and position of the ballast is the same for both surge and pitch motion. However, in the case of Pitch motion, the difference between maximum and minimum RAO peak values is not as significant as for the Surge DOF.

3.3. Cables Response

The cable fairlead tension under the effect of the clump weights was also evaluated. The fairlead is characterized by the higher tension in the cable; thus, using it as comparison quantity is the most conservative condition. Figure 5 shows the RAO of the fairlead tension in the three cables in comparison with a test with no clump weights. The effect of a 5-t weight at 350 m from the platform is presented. Note that a complete assessment of the two design variables is shown later, whereas in Figure 5 only one exemplary combination is considered.

The fairlead tension RAO is positively affected by the clump weight, which is a good indicator in terms of fatigue assessment. The weight seems to not heavily impact the RAO peak (Figure 5a). The position of the ballast (Figure 5b) gives no negligible changes in the fairlead tension at its natural frequency. The peak in the fairlead tension RAO decreases when the distance from the platform becomes smaller, giving its minimum at 50 m from the platform. Figure 5 also shows different behavior between the cables. In particular, the peak amplitude in the upwind cable doubles the ones in the other two cables, while at the second natural frequency there is a decreasing behavior for the upwind cable. This is due to the mooring system layout with cables connected at 120°. This, combined with the fact that the wave motion is aligned with the upwind cable, brings the tension behavior to be the same for the two downwind cables, while the upwind cable becomes the most loaded one.
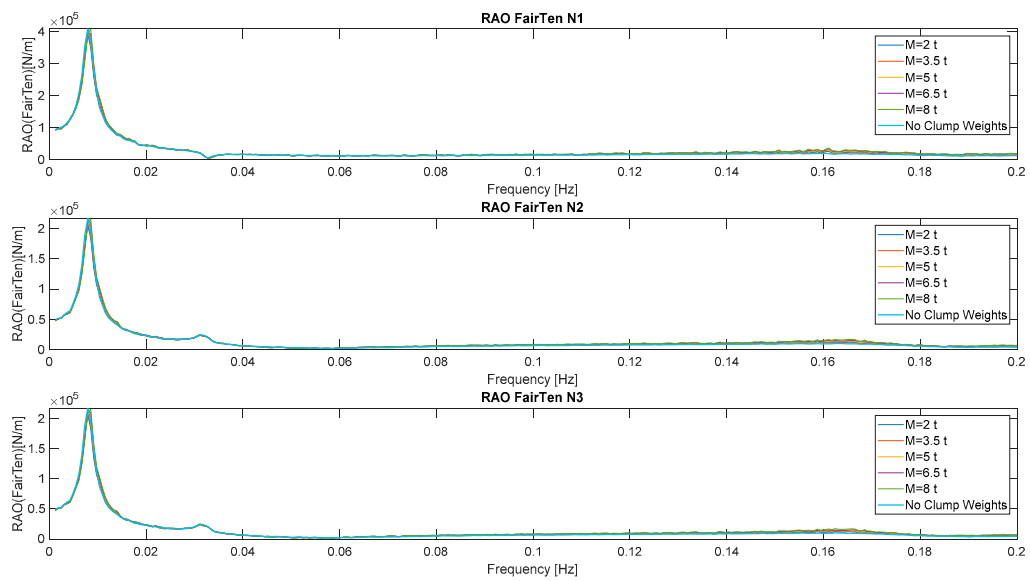
(a)
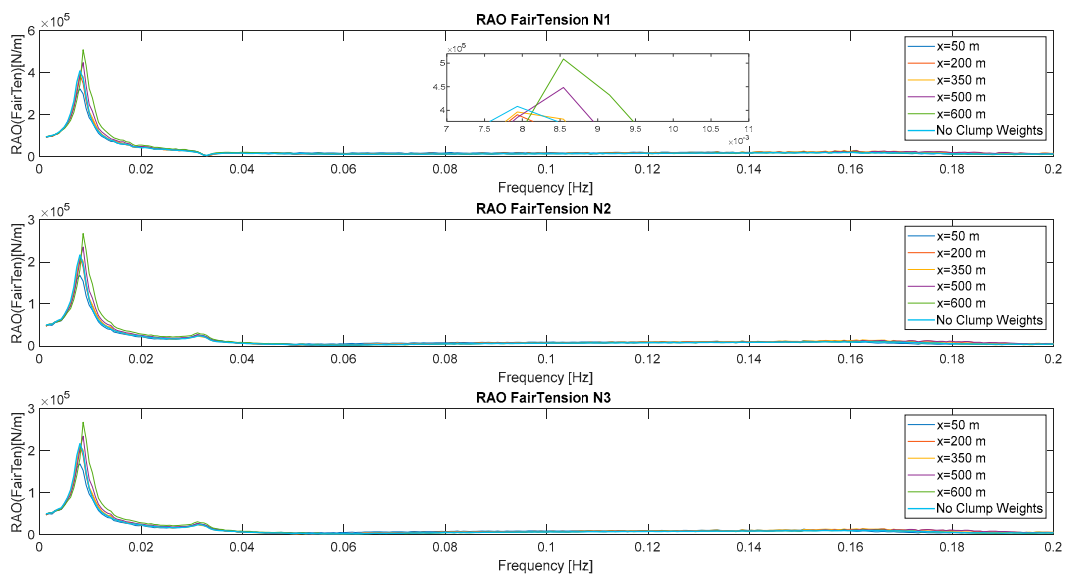
(b)

Figure 5. Fairlead Tension RAOs for different weights (**a**) and positions (**b**) of the cable ballast. Each figure shows the Fairlead Tension for every cable.

Figure 6 shows how the peak of the RAO of the fairlead tension changes with the weight and the position of the ballast. The trend of the fairlead tension is in agreement with the one of the surge RAO peak, showing a minimum for light weights and position close to the platform. Anyway, the value does not change significantly in the lower-left part of the surface, making the position of the ballast the most important variable in this case. However, it is noted that looking only at the RAOs, no information is obtained regarding the mean tension on the cable, which is highly affected by the increase in the cable weight [17].
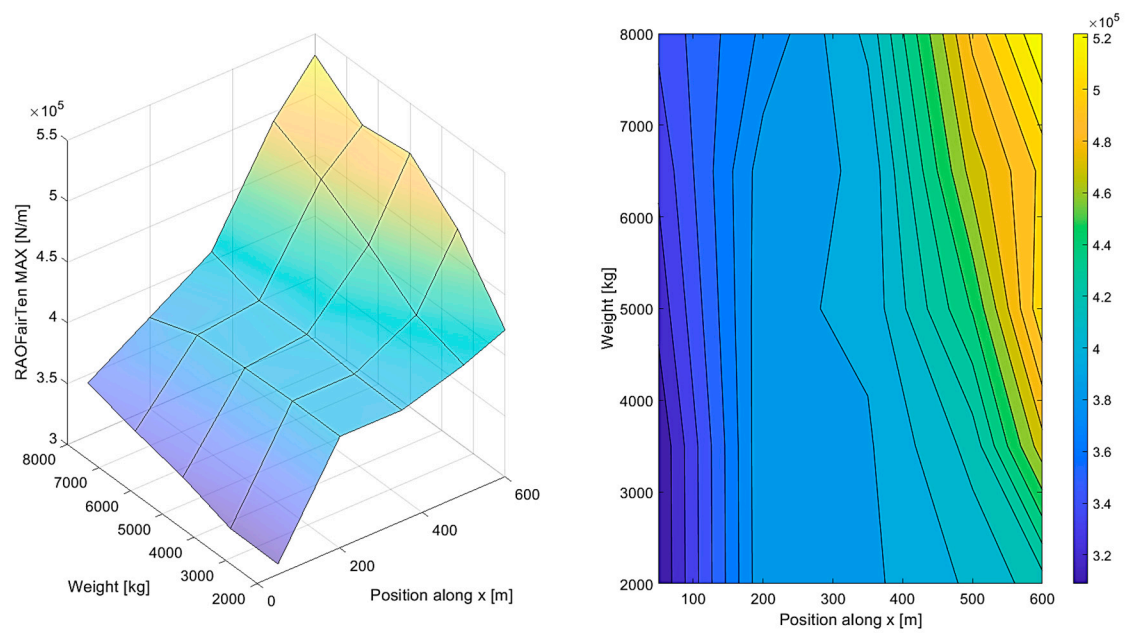
Figure 6. Peak of the Fairlead Tension RAO using 5 different positions and 5 different masses.

Figure 7 shows the mean fairlead tension for the studied cases in comparison with the certified NREL test on the OC3 Hywind without clump weights. It shows a higher tension for heavy ballast, which is expected, and a nonlinear behavior of the tension depending on the position. In fact, the heavier the weight the higher the fairlead tension. It also shown a parabolic behavior in relation to the clump weight position. This is confirmed in Figure 8, where the cable catenary and the tension along the mooring line are shown.
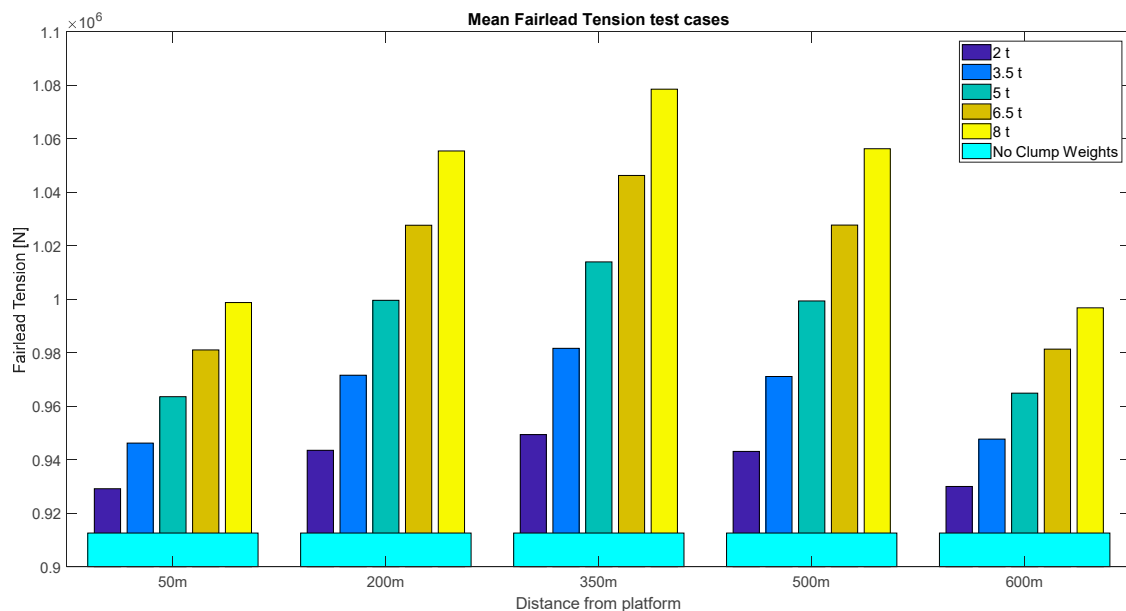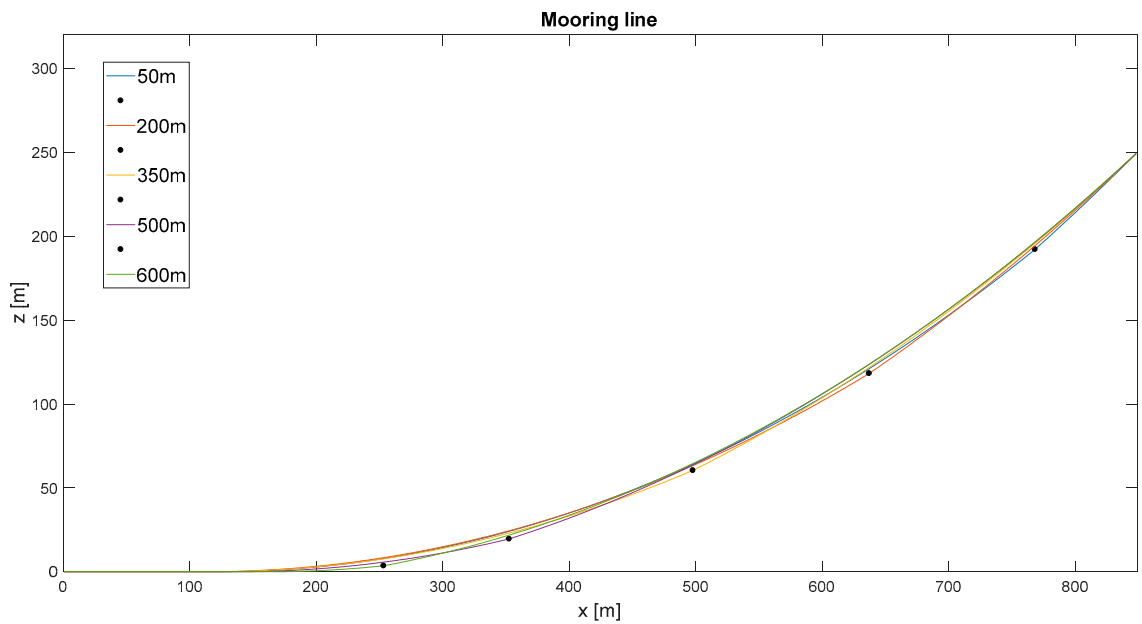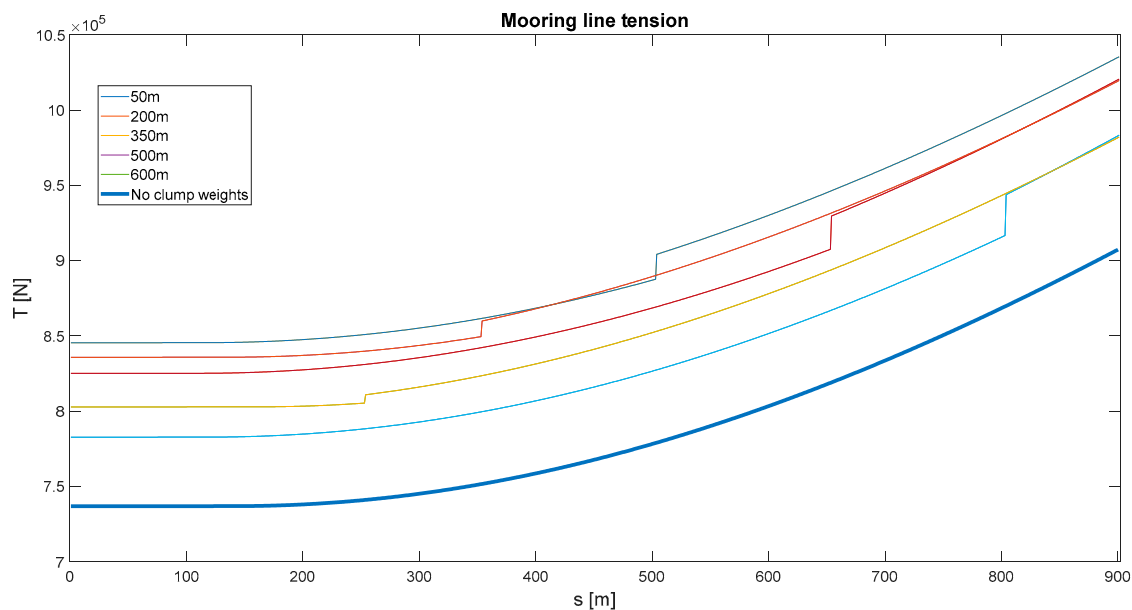

Figure 7. Fairlead mean tension as a function of the weight and the position of the cable ballast.

(**a**) Cable catenary

(**b**) Mooring line mean tension

Figure 8. Cable catenary and mooring line tension depending on the ballast position (M = 5 t).

Figure 8a shows the geometry of the cable adopting a 5-t clump weight in different positions, while Figure 8b shows how the cable mean tension changes with different clump weight positions. The first figure confirms the minimum impact of the clump weight on the geometry of the cable. The latter shows the tension gap at the clump weight position and it decreases with the distance from the platform. It also shows agreement with Figure 7 regarding the fairlead position. Moreover, the clump weight increases the mean tension in the fairlead position about 10% in the optimal range found (50 m, 2 t). The 50-m distance from the platform is shown as a blue catenary in Figure 8b, which is the configuration with the shorter portion of the cable subjected to the higher tension gap. This can lead to adopt a semi-taut cable configuration, which can improve the stiffness of the cable part closer to the platform, while increasing strength-to-weight ratio.

The best configuration in terms of platform response is the one with the weight position at 50 m from the platform. The weight that causes the smallest increase in the cable tension at the fairlead is 2 t. This combination represents the best compromise between benefits and downsides of the clump weight application.

4. Conclusions

The influence of clump weights on the dynamic response of the spar buoy OC3 Hywind platform was investigated in this work. Clump weights positions varying between 50 m and 600 m and their mass varying between 2 tons and 8 tons were considered. The study was focused on the wave-structure interaction with no wind. The system response was evaluated through Response Amplitude Operators (RAOs) obtained using a white noise wave spectrum. This allows to obtain results independent from a specific input (sea-state).

The clump weight mass does not change the platform draft due to the ballast reduction performed at the beginning of the analysis, thus the platform response remains comparable with the one with no clump weights. Results are evaluated considering the RAOs peaks the natural frequencies. RAOs showed a positive influence of the clump weights in the surge motion, while the pitch motion does not gain the same benefit. Surge motion reduces significantly, especially when the ballast is placed close to the platform. This reduction is much more related to the weight position rather than to its mass. Instead, the heavier the ballast, the higher the tension of the cable. This suggests the choice of a lighter ballast and a position closest to the platform in order to maximize benefit in terms of platform response, and, at the same time, to limit the increase in the fairlead tension. These conclusions can lead to new possibilities in the use of semi-taut cables with potential benefits in terms of cable tension and cost.

It should be remarked that RAOs are obtained in absence of wind with the rotor fixed and with a pitch angle of $0°$. Therefore, the aero–servo–elastic effects of the rotor for a turbine in power production were not considered in this phase and should be accounted for in a future study. Moreover, a wider range of design variables, possibly within a multi-objective optimization context, will need to be performed for a more comprehensive study. Moreover, testing the optimal configurations with real sea state and wind parameters would be important to establish the actual impact of the optimization process. These aspects will be addressed in future work.

References

1. Taveira-Pinto, F.; Rosa-Santos, P.; Fazeres-Ferradosa, T. Marine renewable energy. *Renew. Energy* **2020**, *150*, 1160–1164. [CrossRef]
2. Chavez, C.E.A.; Stratigaki, V.; Wu, M.; Troch, P.; Schendel, A.; Welzel, M.; Villanueva, R.; Schlurmann, T.; De Vos, L.; Kisacik, D.; et al. Large-scale experiments to improve monopile scour protection design adapted to climate change—The PROTEUS project. *Energies* **2019**, *12*, 1709. [CrossRef]
3. Walsh, C. Offshore wind in Europe. *Refocus* **2019**, *3*, 14–17. [CrossRef]
4. Robertson, A.N.; Jonkman, J.M. Loads analysis of several offshore floating wind turbine concepts. In Proceedings of the 21st International Offshore and Polar Engineering Conference, Maui, HI, USA, 19–24 June 2011; pp. 443–450.
5. Roddier, D.; Cermelli, C.; Aubault, A.; Weinstein, A. WindFloat: A floating foundation for offshore wind turbines. *J. Renew. Sustain. Energy* **2010**, *2*, 033104. [CrossRef]

6. Jonkman, J. *Definition of the Floating System for Phase IV of OC3 Definition of the Floating System for Phase IV of OC3*; NREL Technical Report NREL/TP-500-47535; National Renewable Energy Laboratory: Golden, CO, USA, 2010. Available online: https://www.nrel.gov/docs/fy10osti/47535.pdf (accessed on 20 February 2020).

7. Karimirad, M.; Moan, T. Feasibility of the application of a spar-type wind turbine at a moderate water depth. *Energy Procedia* **2012**, *24*, 340–350. [CrossRef]

8. Sethuraman, L.; Venugopal, V. Hydrodynamic response of a stepped-spar floating wind turbine: Numerical modelling and tank testing. *Renew. Energy* **2013**, *52*, 160–174. [CrossRef]

9. Utsunomiya, T.; Sato, T.; Matsukuma, H.; Yago, K. Experimental validation for motion of a SPAR-type floating offshore wind turbine using 1/22.5 scale model. *Proc. Int. Conf. Offshore Mech. Arct. Eng. OMAE* **2009**, *4*, 951–959. [CrossRef]

10. Duan, F.; Hu, Z.; Wang, J. Investigation of the VIMs of a spar-type FOWT using a model test method. *J. Renew. Sustain. Energy* **2016**, *8*, 063301. [CrossRef]

11. Adam, F.; Myland, T.; Schuldt, B.; Großmann, J.; Dahlhaus, F. Evaluation of internal force superposition on a TLP for wind turbines. *Renew. Energy* **2014**, *71*, 271–275. [CrossRef]

12. Vita, L.; Ramachandran, G.K.V.; Krieger, A.; Kvittem, M.I.; Merino, D.; Cross-Whiter, J.; Ackers, B.B. Comparison of numerical models and verification against experimental data, using Pelastar TLP concept. In Proceedings of the International Conference on Offshore Mechanics and Arctic Engineering OMAE, St. John's, NL, Canada, 31 May–5 June 2015; pp. 1–11. [CrossRef]

13. Karimirad, M.; Michailides, C. V-shaped semisubmersible offshore wind turbine: An alternative concept for offshore wind technology. *Renew. Energy* **2015**, *83*, 126–143. [CrossRef]

14. Robertson, H.S.A.; Jonkman, J.; Masciola, M. *Definition of the Semisubmersible Floating System for Phase II of OC4*; Technical Report NREL/TP-5000-60601; National Renewable Energy Laboratory: Golden, CO, USA, 2014. Available online: https://www.nrel.gov/docs/fy14osti/60601.pdf (accessed on 20 February 2020).

15. Chen, D.; Gao, P.; Huang, S.; Fan, K.; Zhuang, N. Dynamic response and mooring optimization of spar-type substructure under combined action of wind, wave, and current. *J. Renew. Sustain. Energy* **2017**, *9*, 063307. [CrossRef]

16. Driscoll, F.; Jonkman, J.; Robertson, A.; Sirnivas, S.; Skaare, B. Validation of a FAST model of the statoil-hywind demo floating wind turbine. *Energy Procedia* **2016**, *94*, 3–19. [CrossRef]

17. Liu, Z.; Tu, Y.; Wang, W.; Qian, G. Numerical analysis of a catenary mooring system attached by clump masses for improving the wave-resistance ability of a spar buoy-type floating offshore wind turbine. *Appl. Sci.* **2019**, *9*, 1075. [CrossRef]

18. Hegseth, J.M.; Bachynski, E.E.; Martins, J.R.R.A. Design optimization of spar floating wind turbines considering different control strategies. *Mar. Struct.* **2020**, *72*, 102771. [CrossRef]

19. Muskulus, M.; Schafhirt, S. Design optimization of wind turbine support Structures—A Review. *J. Ocean. Wind Energy* **2014**, *1*, 12–22.

20. Jonkman, J.M.; Buhl, M.L., Jr. *FAST User's Guide*; National Renewable Energy Laboratory: Golden, CO, USA, 2005.

21. Larsen, T.; Hansen, A. *How 2 HAWC2, the User's Manual*; Risø DTU National Laboratory: Roskilde, Denmark, 2015; Volume 2.

22. Barbanti, G.; Marino, E.; Borri, C. Mooring system optimization for a spar-buoy wind turbine in rough wind and sea conditions. *Lect. Notes Civ. Eng.* **2019**, *27*, 87–98. [CrossRef]

23. Yuan, Z.; Incecik, A.; Ji, C. Numerical study on a hybrid mooring system with clump weights and buoys. *Ocean. Eng.* **2014**, *88*, 1–11. [CrossRef]

24. Hordvik, T. *Design Analysis and Optimisation of Mooring System for Floating Wind Turbines*; Norges Teknisk-Naturvitenskapelige Universitet, Fakultet for Ingeniørvitenskap og Teknologi, Institutt for Marin Teknikkm: Trondheim, Norway, 2011.

25. Morison, J.R.; Johnson, J.W.; O'Brien, M.P. Experimental studies of forces on piles. *Coast. Eng. Proc.* **2000**, *1*, 25. [CrossRef]

26. Jonkman, J.; Butterfield, S.; Musial, W.; Scott, G. Definition of a 5-MW reference wind turbine for offshore system development. *Am. J. Med. Genet.* **2009**, *107*, 317–324. [CrossRef]

27. Robertson, A.N.; Wendt, F.; Fonkman, J.M.; Popko, W.; Dagher, H.; Gueydon, S.; Qvist, J.; Vittori, F.; Uzunoglu, E.; Harries, R.; et al. OC5 project phase II: Validation of global loads of the deepcwind floating semisubmersible wind turbine. *Energy Procedia* **2017**, *137*, 38–57. [CrossRef]

28. Hall, M. *MoorDyn User's Guide*; Department of Mechanical Engineering, University of Maine: Orono, ME, USA, 2017.

29. Hall, M.; Buckham, B.; Crawford, C. Evaluating the importance of mooring line model fidelity in floating offshore wind turbine simulations. *Wind Energy* **2013**, *17*, 1835–1853. [CrossRef]

30. Wendt, F.; Robertson, A.; Jonkman, J.; Hayman, G. Verification of New Floating Capabilities in FAST v8 Preprint. In Proceedings of the 33rd Wind Energy Symposium, Proc AIAA SciTech 2015, Kissimmee, FL, USA, 5–9 January 2015; p. 1204.

31. Jonkman, J.M.; Robertson, A.N.; Hayman, G.J. *HydroDyn User's Guide and Theory Manual HydroDyn User's Guide and Theory Manual*; National Renewable Energy Laboratory: Golden, CO, USA, 2014.

32. Matha, D.; Schlipf, M.; Pereira, R. Challenges in Simulation of Aerodynamics, Hydrodynamics, and Mooring-Line Dynamics of Floating Offshore Wind Turbines. In Proceedings of the 21st International Offshore and Polar Engineering Conference, Maui, HI, USA, 19–24 June 2011.

33. WAMIT Inc. Wamit user manual. *J. Chem. Inform. Model.* **2013**, *53*, 1689–1699.

34. Marino, E.; Lugni, C.; Borri, C. The role of the nonlinear wave kinematics on the global responses of an OWT in parked and operating conditions. *J. Wind Eng. Ind. Aerodyn.* **2013**, *123*, 363–376. [CrossRef]

35. Paulsen, B.T.; Bredmose, H.; Bingham, H.B.; Jacobsen, N.G. Forcing of a bottom-mounted circular cylinder by steep regular water waves at finite depth. *J. Fluid Mech.* **2014**, *755*, 1–34. [CrossRef]

36. Marino, E.; Giusti, A.; Manuel, L. Offshore wind turbine fatigue loads: The influence of alternative wave modeling for different turbulent and mean winds. *Renew. Energy* **2017**, *102*, 157–169. [CrossRef]

37. Mockute, A.; Marino, E.; Lugni, C.; Borri, C. Comparison of nonlinear wave-loading models on rigid cylinders in regular waves. *Energies* **2019**, *12*, 4022. [CrossRef]

38. Marino, E.; Lugni, C.; Borri, C. A novel numerical strategy for the simulation of irregular nonlinear waves and their effects on the dynamic response of offshore wind turbines. *Comput. Methods Appl. Mech. Eng.* **2013**, *255*, 275–288. [CrossRef]

39. Marino, E.; Borri, C.; Peil, U. A fully nonlinear wave model to account for breaking wave impact loads on offshore wind turbines. *J. Wind Eng. Ind. Aerodyn.* **2011**, *99*, 483–490. [CrossRef]

40. Chuang, Z.; Liu, S.; Lu, Y. Influence of second order wave excitation loads on coupled response of an offshore floating wind turbine. *Int. J. Nav. Archit. Ocean. Eng.* **2020**, *12*, 367–375. [CrossRef]

41. Orszaghova, J.; Taylor, P.H.; Wolgamot, H.; Madsen, F.J.; Bredmose, H. Second and third order sub-harmonic wave responses of a floating wind turbine. In Proceedings of the 35th International Work, Water Waves and Floating Bodies, Seoul, Korea, 24–28 August 2020; pp. 26–29.

42. Xu, K.; Shao, Y.; Gao, Z.; Moan, T. A study on fully nonlinear wave load effects on floating wind turbine. *J. Fluids Struct.* **2019**, *88*, 216–240. [CrossRef]

43. Xu, K.; Zhang, M.; Shao, Y.; Gao, Z.; Moan, T. Effect of wave nonlinearity on fatigue damage and extreme responses of a semi-submersible floating wind turbine. *Appl. Ocean. Res.* **2019**, *91*, 101879. [CrossRef]

44. Ferri, G.; Marino, E.; Borri, C. Optimal dimensions of a semisubmersible floating platform for a 10 MW wind turbine. *Energies* **2020**, *13*, 3092. [CrossRef]

45. Hegseth, J.M.; Bachynski, E.E. A semi-analytical frequency domain model for efficient design evaluation of spar floating wind turbines. *Mar. Struct.* **2019**, *64*, 186–210. [CrossRef]

46. Faltinsen, O.M.; Michelsen, F.C. *Motions of Large Structures in Waves at Zero Froude Number*; Det Norske Veritas: Oslo, Norway, 1975; pp. 2–18.

47. Ramachandran, G.K.V.; Robertson, A.; Jonkman, J.M.; Masciola, M.D. Investigation of response amplitude operators for floating offshore wind turbines. In Proceedings of the 23rd International Ocean, Offshore and Polar Engineering Conference, Anchorage, AK, USA, 30 June–5 July 2013; pp. 369–376.